

## Preparation and characterization of poly (styrene-acrylonitrile) (SAN)/clay nanocomposites by melt intercalation

Yibing Cai · Yuan Hu · Shanyong Xuan ·  
Yi Zhang · Huaxia Deng · Xinglong Gong ·  
Zuyao Chen · Weicheng Fan

Received: 29 July 2006 / Accepted: 28 September 2006 / Published online: 3 April 2007  
© Springer Science+Business Media, LLC 2007

**Abstract** Poly (styrene-acrylonitrile) (SAN)/clay nanocomposites have been prepared by melt intercalation method from pristine montmorillonite (MMT), using hexadecyl trimethyl ammonium bromide (C16) and hexadecyl triphenyl phosphonium bromide (P16) as the reactive compatibilizers between polymer and clay. The influence of the reactive compatibilizers proportion relative to the clay on the structure and properties of the SAN/clay nanocomposites is investigated by X-ray diffraction (XRD) and transmission electron microscopy (TEM), high-resolution electron microscopy (HREM), thermogravimetric analysis (TGA) and dynamic mechanical analysis (DMA). The effects of the two different clays (MMT and organic modified MMT) on the nanocomposites formation, morphology and property are also studied. The results indicate that the SAN cannot intercalate into the interlayers of the MMT and results in microcomposites. In the presence of the reactive compatibilizers, the dispersion of clay in SAN is rather facile and the SAN/clay nanocomposites reveal an intermediate morphology, an intercalated structure with some exfoliation and the presence of small tactoids. The

appropriate proportion with 3 wt% reactive compatibilizers to 5 wt% MMT induces well-dispersed morphology and properties in the SAN matrix. The TGA analyses show that the thermal stability properties of the SAN/clay nanocomposites have been improved compared with those of the pristine SAN. The DMA results show that the storage modulus and glass transition temperature ( $T_g$ ) of the SAN/clay nanocomposites have remarkably enhancements compared with the pristine SAN. At last the intercalation mechanism of the technology is discussed.

### Introduction

Polymer-layered silicate clay nanocomposites, as a very promising alternative to conventional filled polymers, have attracted considerable attention of academic and industrial researchers in recent decades. The dispersion of these ultra-thin (1 nm) ultra-high surface-area clay layers (usually less than 10 wt%) within a polymer matrix leads to nanocomposites exhibiting markedly improved physicochemical properties, better dimensional and thermal stabilities, improved gas barrier properties and reduced flammability, compared with pristine polymers or conventional microcomposites. In general, polymer-layered silicate composites are of three categories: microcomposites, exfoliated composites and intercalated composites. Many of the properties associated with polymer-layered silicate nanocomposites are a function of the extent of exfoliation of the individual clay sheets. Among these enhanced properties, mechanical and gas barrier properties are related to the types of clay dispersion in the polymer, while fire retardant property has been ascribed to the formation of a barrier

---

Y. Cai · Y. Hu (✉) · S. Xuan · Y. Zhang ·  
W. Fan  
State Key Laboratory of Fire Science, University of Science and  
Technology of China, Hefei 230026 Anhui, P.R. China  
e-mail: yuanhu@ustc.edu.cn

H. Deng · X. Gong  
CAS Key Laboratory of Mechanical Behavior and Design of  
Materials, Department of Mechanics and Mechanical  
Engineering, University of Science and Technology of China,  
Hefei 230027, P.R. China

Z. Chen  
Department of Chemistry, University of Science and Technology  
of China, Hefei 230026 Anhui, P.R. China

which impedes mass transport of degrading polymer species and insulates the flame from the underlying polymer [1–6].

Poly (styrene-acrylonitrile) (SAN) is a widely used engineering thermoplastic owing to its desirable properties, which include good mechanical properties, chemical resistance and easy processing characteristics. It has many important applications, such as the fittings of mobile industry and home appliance, instrument panel, various switches and lamina of the fanner, etc. Furthermore, SAN is the matrix phase of the multiphase ABS. Therefore the studies of SAN-layered silicate nanocomposites have very important significance and can be served as a simple and useful model for understanding the more complex ABS-layered silicate nanocomposites system. To date, there are numerous literatures reported the SAN-layered silicate nanocomposites. Chu et al. [7] studied the effect of clay organic treatment and AN content on SAN nanocomposites formation and flammability. The results showed that the stronger the polar of organic treatment was, the better the clay dispersion was and SAN with higher AN content gave better dispersions with most of the clays studied. Bourbigot et al. [8] investigated the influence of the clay on mechanical properties and fire performance of SAN. At the same time, the nanodispersion was evaluated quantitatively by solid state NMR. The results showed that the presence of clay led to a “filler effect” which made the stiffness increase, the tensile strength decrease and PHRR decrease significantly. Bok et al. [9] studied the effects of clay on the thermal degradation behavior of SAN by GC-MS. The virgin SAN degraded via chain scission followed by  $\beta$ -scission, producing monomers, dimmers and trimers. The degradation of SAN in clay nanocomposites contained additional steps, including extensive random chain scission and radical recombination. The studies of Stretz et al. [10] indicated that SAN/MMT nanocomposites effectively modeled the organoclay dispersion seen in more complex ABS/MMT nanocomposites. The results showed that the clay particles in a drop-in melt-processed ABS formulation resided in the SAN matrix phase, with some accumulation of MMT particles at the rubber surface, which seemed to conform to the rubber particle shape. Kim et al. [11, 12] synthesized the SAN/clay nanocomposites by emulsion polymerization and studied the electrorheological (ER) behavior. The intercalated particles were used for ER fluid, showing typical ER behavior such that both yield stress and enhanced shear stress were observed as functions of applied electric field and shear rate. Wang et al. [13] synthesized the SAN/clay nanocomposites by free radical polymerization and investigated the dielectric properties. The dielectric loss increased as clay loading increased. The ICP experiments approved the reason, which thought to be related to the sodium content in the clay.

Based on the above literatures reviews, the studying the organic treatment effects on polymer nanocomposites formation and properties is highly important, as the organic treatment is the interface between layered silicate and polymer. A poor interface between polymer and layered silicate will often result in a microcomposites, or a traditional filled system. Hence, the study of different organic treatment on the clay surface can help us understand how this interface affects the properties observed in the final polymer layered-silicate nanocomposites, as well as how that organic treatment gives rise to the observed nanocomposites structure. In this paper, we report the use of two different approaches to synthesize poly (styrene-acrylonitrile) (SAN)/clay nanocomposites by melt intercalation [14]. With this method, two different cationic surfactants, alkyl quaternary ammonium salt (C16) and alkyl quaternary phosphonium salt (P16) bearing long alkyl chain, are used as the SAN reactive compatibilizers. At the same time, it should be noted that two different layered silicates are also used for this work: the pristine clay (montmorillonite, MMT) and the organophilic montmorillonite (OMT). The objective of this work is to investigate the influence of the two different clays and reactive compatibilizers on the nanodispersion of the clay, thermal stability and mechanical property in SAN matrix. The paper provides a simple process technique for manufacturing SAN/clay nanocomposites with improved thermal stability and mechanical properties by direct melt intercalation.

## Experimental

### Materials

Poly (styrene-acrylonitrile) (SAN, 32.5–34.5 wt% AN) was supplied as pellets by the Guoheng Chemical Company (Zhenjiang China). The pristine montmorillonite (MMT), with a cation exchange capacity (CEC) of 97 meq/100 g was kindly provided by Keyan Company. Hexadecyl trimethyl ammonium bromide (C16) and hexadecyl triphenyl phosphonium bromide (P16) were obtained from Shanghai Chemistry Company and Jintan Xinan Chemical Institute (Jiangsu China), respectively.

The preparation of organophilic montmorillonite (OMT)

Organophilic montmorillonite (OMT) was prepared by cation exchange of natural counterions with ammonium cationic surfactant according to the method of Kawasumi et al. [15]. The alkyl quaternary ammonium salts used were hexadecyl trimethyl ammonium bromide (C16). The MMT and OMT were dried under vacuum at 80 °C for several

hours before use. The interlayer spacing for pristine MMT and OMT was measured by X-ray diffraction.

#### The preparation of SAN/clay nanocomposites

The preparation of SAN/clay nanocomposites followed two different methods. The conventional method [16] was used. The pellets of SAN and MMT, OMT were melt blended using a twin-roll mill (XK-160, Jiangsu, China) to yield the hybrids. The second method was also used in present work. Firstly, the pristine MMT (dried powder) and C16 or P16 were mixed (the weight ratio of MMT/C16 or P16 is shown in Table 1) and ground together in a mortar and pestle. Then the mixed powder (the weight ratio of MMT + C16 or P16) and SAN was melt-mixed in twin-roll mill. The temperature of the mill was maintained at 180 °C and the roll speed was maintained at 100 rpm. The resulting samples were compressed and moulded into sheets (1 mm and 3 mm thickness). The samples are listed in Table 1.

#### Characterization

X-ray diffraction (XRD) patterns were performed on the 1 mm thick films with a Japan Rigaku D/Max-Ra rotating anode X-ray diffractometer (30 kV, 10 mA) with Cu ( $\lambda = 1.54 \text{ \AA}$ ) irradiation at a rate of 20/min in the range of 1.5–10°.

Transmission electron microscopy (TEM) images were obtained on a Jeol JEM-100SX transmission electron microscope with an acceleration voltage of 100 kV. High-resolution electron microscopy (HREM) images were obtained by JEOL 2010 with an acceleration voltage of 200 kV. The TEM and HREM specimens were cut at room temperature using an ultramicrotome (Ultracut-1, UK) with a diamond knife from an epoxy block with the films of the nanocomposite embedded. Thin specimens, 50–80 nm, were collected in a trough filled with water and placed on 200 mesh copper grids.

Thermogravimetric analyses (TGA) were conducted with a Netzsch STA 409C thermo-analyzer instrument. In each case, the about 10 mg specimens were heated from 25 °C to 700 °C using a linear heating rate of 10 °C/min under nitrogen flow.

The dynamic mechanical measurements of materials were carried out using a Tritec 2000B Dynamic Mechanical Analyser from 30 °C to 180 °C with a heating rate of 5 °C/min under 0.04% of deformation at 1 Hz of frequency. The samples (dimension 15 mm × 9 mm × 1 mm) were molded in 180 °C for 10 min under 5 Mpa of pressure.

## Results and discussion

### Effect of clay types on the SAN nanocomposites

The effects of the two different clays (MMT and OMT) on the structure and properties of the SAN nanocomposites are studied. The compositions of the samples are listed in Table 1. The structure, thermal stability and mechanical properties are analyzed by XRD, TEM, HREM, TGA and DMA, respectively. The data of XRD are listed in Table 2. Figure 1 shows the XRD curves of MMT and the corresponding SAN nanocomposites. The peaks correspond to the (001) reflections of the clay. The  $d_{001}$  peak of the pristine MMT at  $2\theta = 5.8^\circ$  corresponds to 1.51 nm interlayer spacing. Then the SAN2 (containing MMT) exhibits only a weak diffraction peak corresponding to an interlayer spacing of the pristine MMT. The results indicate that the SAN matrix cannot intercalate into the pristine MMT interlayer and results in microcomposites. The reasons may be that the pristine MMT is hydrophilic and the SAN matrix is hydrophobic, so that it is hard to obtain a thermodynamically homogeneous mixture of clay with SAN matrix on the molecular level. The TEM results also suggest that the clay

**Table 1** Formulations of SAN/clay nanocomposites

Sample	Clay (wt%)	Reactive compatibilizer (wt%)
SAN1	Pristine SAN	
SAN2	MMT(5)	
SAN3	OMT(5)	
SAN4	MMT(5)	C16(1)
SAN5	MMT(5)	C16(3)
SAN6	MMT(5)	C16(5)
SAN7	MMT(5)	P16(1)
SAN8	MMT(5)	P16(3)
SAN9	MMT(5)	P16(5)

**Table 2** The data of XRD for SAN/clay nanocomposites. Sample refers to the number of formulation in Table 1

Sample code	d (nm)	$\Delta d$ (nm)
MMT	1.51	
OMT	2.39	
SAN2	1.51	0
SAN3	3.15	0.76
SAN4	3.18	1.67
SAN5	3.43	1.92
SAN6	3.54	2.03
SAN7	3.33	1.82
SAN8	3.67	2.16
SAN9	4.10	2.59

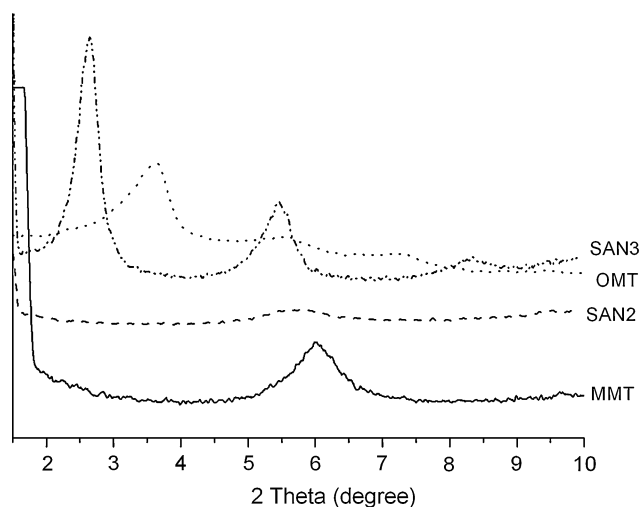
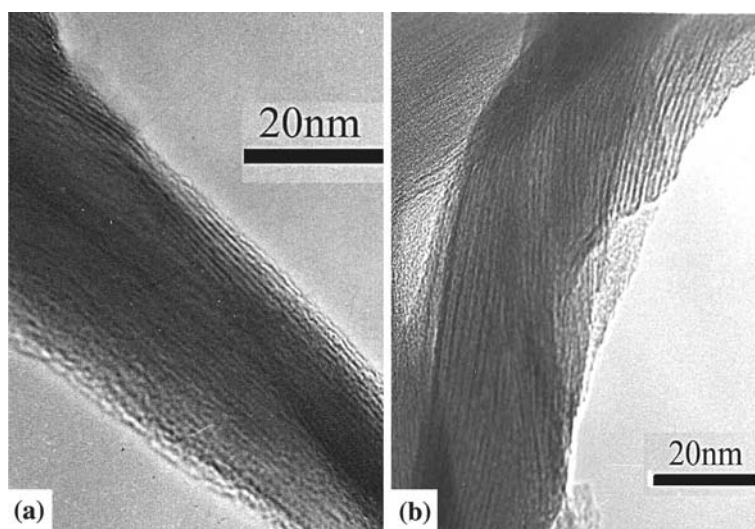


**Fig. 1** The XRD curves of MMT, OMT and the corresponding SAN/clay nanocomposites

agglomerates in  $\mu\text{m}$ -size are distributed in SAN (Fig. 3a). This result accords with the XRD analysis.

The typical method to increase the compatibility of clay with polymer is to block hydrophilic functional groups on the surface or attach organic molecules of long hydrocarbon tails on the surface. Therefore, the organic modified MMT (OMT) is prepared by cation exchange of natural counterions with hexadecyl trimethyl ammonium bromide (C16). The XRD analysis indicates that the  $d_{001}$  peak of the OMT, the corresponding interlayer spacing of which is 2.39 nm (Fig. 1), is observed at lower angle ( $2\theta = 3.7^\circ$ ) than that of the pristine MMT. The results indicate the ammonium ions intercalate into the silicate layers and expand the basal spacing of clay. The HREM photograph of the MMT and OMT is shown in Fig. 2. The image indicates that the MMT (Fig. 2a) consists of lamellar structure and the OMT (Fig. 2b) still retains the kind of

**Fig. 2** The HREM images of MMT and OMT

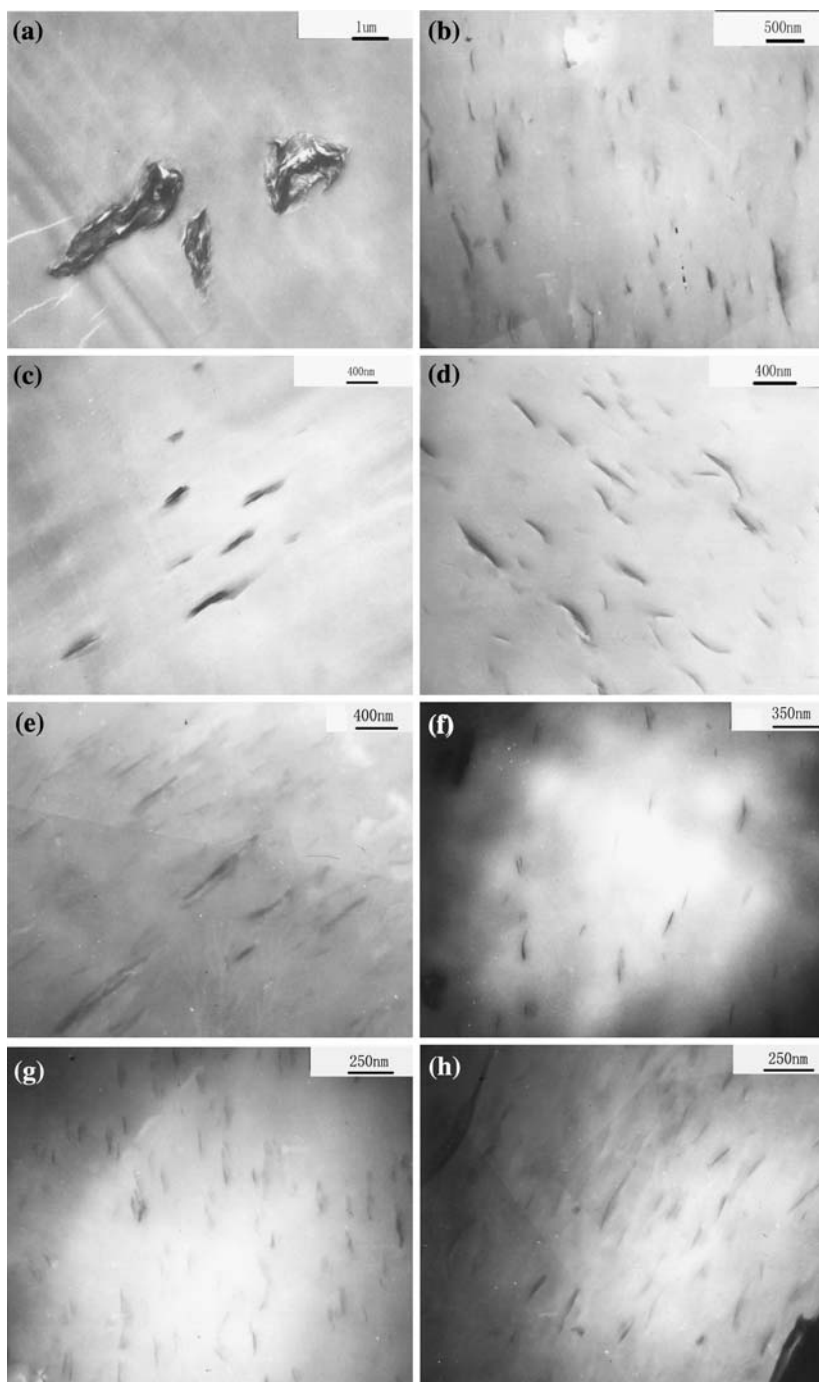


lamellar structure. The crystal structure is not destroyed. At the same time, the XRD results show that the SAN3 (containing OMT) nanocomposites has an increase in the interlayer spacing of the clay. There is 0.76 nm gallery height increase compared to that of the OMT. The results indicate that an intercalated structure is formed in the SAN3 and show that this cationic surfactant is a good one for interface with SAN matrix, allowing polymer intercalation to occur. The intercalated morphology are confirmed by the TEM and HREM photographs. The silicate layers are well dispersed in SAN matrix and some tactoids (multiplayer particles) are visible (Figs. 3b, 4a).

Thermal stability for which the polymer/clay nanocomposites morphology plays an important role is an important property. The TGA curves for the SAN/clay nanocomposites are shown in Fig. 5. The TGA results of the 5% weight loss temperature ( $T_{-5 \text{ wt\%}}$ ), the half weight loss temperature ( $T_{-50 \text{ wt\%}}$ ) and char residue at 700 °C are listed in Table 3. As far as  $T_{-5 \text{ wt\%}}$  and  $T_{-50 \text{ wt\%}}$  are concerned, there are not distinct difference between SAN1 and SAN2. The  $T_{-5 \text{ wt\%}}$  and  $T_{-50 \text{ wt\%}}$  of SAN3 nanocomposites are lower and higher than those of pristine SAN matrix or SAN2 microcomposites, respectively. The reason of the  $T_{-5 \text{ wt\%}}$  temperature decrease may be that the cationic surfactant degrades in advance. The increase of the  $T_{-50 \text{ wt\%}}$  temperature is attributed to the formed nanocomposites and the barrier property of silicate clay layers. The amount of the char residue has a certain degree enhancement, contributing to the improved thermal stability.

The dynamic mechanical behaviors of the SAN/clay nanocomposites are studied (Figs. 6, 7). The storage modulus of the SAN2 at 30 °C decreases slightly compared with the pristine SAN, due to the clay dispersion poorly. The incorporation of 5 wt% OMT to SAN (SAN3) produces a 44% increase in storage modulus at 30 °C. The tactoids and individual layers are incapable of freely

**Fig. 3** TEM images of SAN/clay nanocomposites (a) SAN2, (b) SAN3, (c) SAN4, (d) SAN5, (e) SAN6, (f) SAN7, (g) SAN8 and (h) SAN9



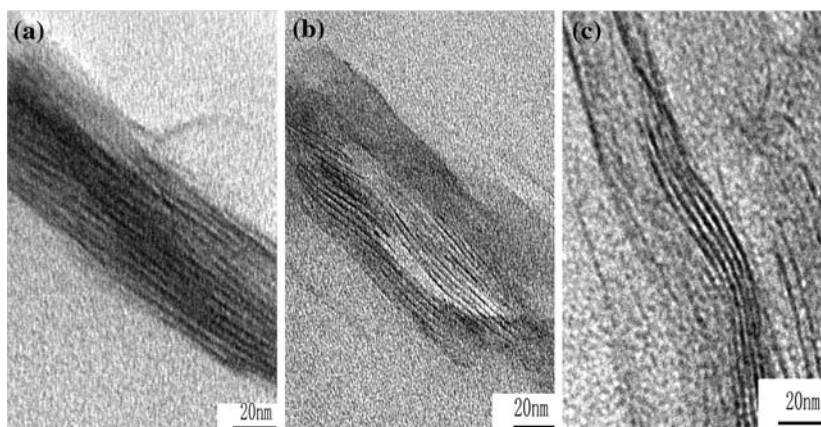
rotating, and are prevented from relaxing completely. The incomplete relaxation due to physical jamming or percolating leads to the solidlike behavior and causes the increase of storage modulus [6]. The glass transition temperature ( $T_g$ ) of each nanocomposites is obtained from the maximum temperature of  $\tan \delta$  in Fig. 7. The  $T_g$  of the SAN1, SAN2 and SAN3 is 108 °C, 111 °C and 113 °C, respectively. The increase of  $T_g$  obtained from those SAN/clay nanocomposites is mainly due to the SAN copolymers intercalate into the silicate layers of clay, the confined

polymer chains in clay galleries are not completely free and the consequence of the increased thermal insulation effect of clay [12, 17].

Effect of the two different reactive compatibilizers and its loadings on clay dispersion and thermal stability in SAN

The effects of the two different reactive compatibilizers and its proportion relative to the clay on SAN/clay nano-

**Fig. 4** The HREM images of (a) SAN3, (b) SAN5 and (c) SAN8



composites are studied. The detailed compositions of the formulations are listed in Table 1. Each of these formulations is analyzed by XRD, TGA, TEM and HREM analysis to determine what type of nanocomposites is obtained. The XRD curves are shown in Fig. 8. The SAN nanocomposites (containing MMT and reactive compatibilizers) show a significant amount of interlayer spacing increase compared to that of MMT. The data of XRD for these formulations are summarized in Table 2. The results indicate that an intercalated structure is formed in the SAN matrix and the reactive compatibilizers improve the interface adhesion and decrease the interfacial energy between the MMT and SAN matrix, allowing polymer intercalation to occur. Interestingly, there appears to be an increase of interlayer spacing with the increase of the reactive compatibilizer loadings. Maybe the excessive reactive compatibilizers intercalates also into the interlayers of the pristine MMT. Furthermore, the MMT with P16 always show an interlayer spacing increase more than that of the MMT with C16. The reason for this is that the molecular dimension of the P16 is larger than that of the C16.

Figures 3 and 4 show the TEM and HREM images of the SAN/clay nanocomposites. The TEM microscopy

results for the formulations of SAN/MMT/C16 (Fig. 3c, d, e) and SAN/MMT/P16 (Fig. 3f, g, h) nanocomposites show that the distribution of silicate layers is generally uniform. These nanocomposites exhibit very good clay dispersion. The reasons may be that the formulation is a dynamically reactive process during melt-mixed. The prominent interaction will arise among the three components of the formulation: the silicate layer surface, the cationic surfactant chains (C16 or P16) and the polymer matrix. At first, some surfactant chains diffuse into the clay interlayer by physical absorption and mechanical shear. Because the negative charge originates in the silicate layer, the cationic head group of the cationic surfactant will preferentially reside in the silicate layer surface and the aliphatic tail will radiate away from the surface. In fact, this course just makes the pristine MMT organophilic, which will reduce the interfacial energies. However, there are some differences in this formulation because the cationic surfactant does not entirely diffuse into the interlayer at the same time. It means that there is some cationic surfactants stay at the polymer matrix (SAN), which may enhance the compatibility between the SAN matrix and the MMT interlayer. At the same time, there is also an interaction between the polymer

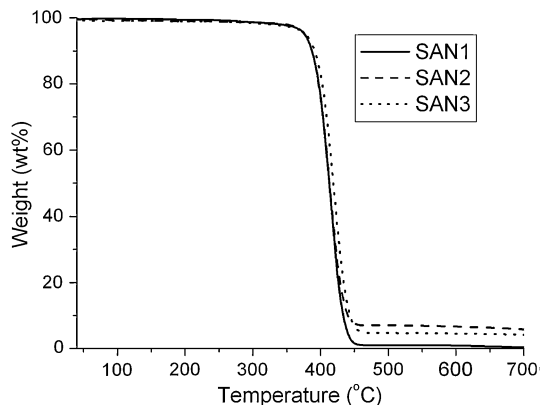


**Fig. 5** The TGA curves for SAN1, SAN2 and SAN3

**Table 3** The data of TGA for SAN/clay nanocomposites. Sample refers to the number of formulation in Table 1

Sample code	T <sub>-5 wt%</sub> (°C)	T <sub>-50 wt%</sub> (°C)	Char residue (700 °C)
SAN1	381.3	413.7	0.37
SAN2	381.1	413.8	5.84
SAN3	378.4	419.4	4.18
SAN4	378.3	416.3	5.53
SAN5	363.0	418.5	6.28
SAN6	316.1	415.9	9.76
SAN7	376.3	415.7	5.15
SAN8	373.5	419.8	6.45
SAN9	358.7	416.2	11.82

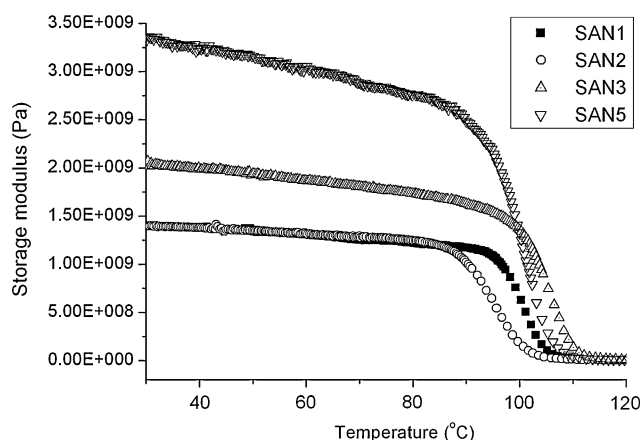


**Fig. 6** Storage modulus of the SAN-clay nanocomposites for SAN1, SAN2, SAN3 and SAN5

matrix and the cationic surfactant, just like the interaction between the cationic surfactant and the silicates clay [18–20]. Both the SAN/MMT/C16 and the SAN/MMT/P16 nanocomposites give well-dispersed clay dispersion, but the clay plate dimension is different. The clay plate sizes of the SAN/MMT/P16 series nanocomposites are much slender than those of the corresponding SAN/MMT/C16 series nanocomposites. This is because the phenyl structure of the P16 is similar with the SAN matrix and results in better compatibility compared with the C16. Furthermore, the clay plate sizes decrease firstly and then increase slightly with the increase of the reactive compatibilizers loadings. When the reactive compatibilizer loading is 3 wt% relative to the 5 wt% MMT, the clay plate sizes arrive at the minimum (Fig. 3d, g). Then, when the reactive compatibilizer content increases up to 5 wt%, the MMT clay (Fig. 3e, h) begins to agglomerate and the dispersion degree of clay descends in the SAN matrix. It is concluded that the intercalation into the silicate clay interlayer is not only SAN but also the excessive reactive compatibilizers.

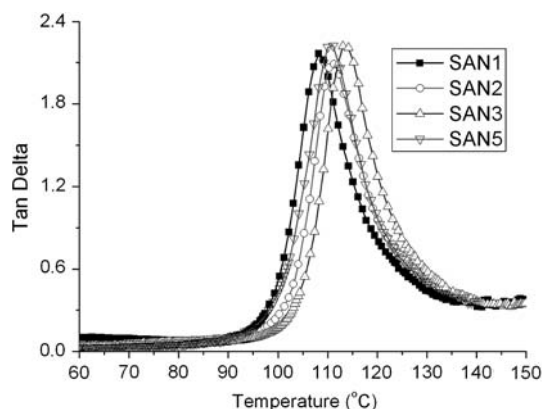


**Fig. 7** Tan  $\delta$  curves of the SAN/clay nanocomposites for SAN1, SAN2, SAN3 and SAN5

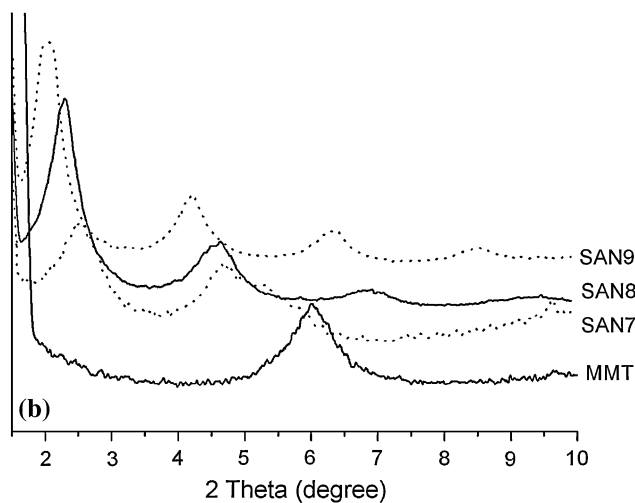
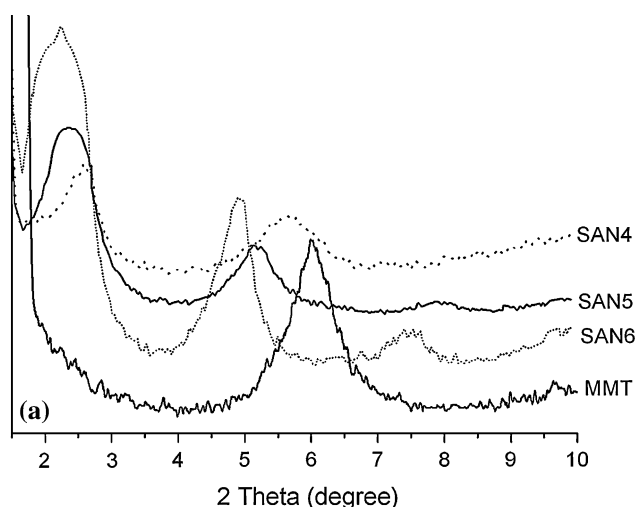


**Fig. 8** The XRD curves of MMT and the corresponding SAN/MMT/C16 (a) and SAN/MMT/P16 (b) nanocomposites

This result accords with the reported results in literatures [18, 21–24], which shows the amount of the MMT and the reactive compatibilizer have an appropriate proportion.

The HREM images of SAN/clay nanocomposites are shown in Fig. 4. The HREM microscopy for SAN/MMT/C16 (SAN5, Fig. 4b) and SAN/MMT/P16 (SAN8, Fig. 4c) with 3 wt% reactive compatibilizers shows that silicate layer distribution is generally uniform where a fraction of aggregates containing only several silicate layers are observable. This mesostructure can be taken as a delaminated–intercalated nanocomposites. Moreover, the clay plate height of SAN/MMT/P16 is slimmer than that of the SAN/MMT/C16. This result is the same as the TEM investigation.

The thermal stability of the SAN/MMT/C16 series nanocomposites and SAN/MMT/P16 series nanocomposites are analyzed by TGA. The TGA curves are shown in Figs. 9 and 10, respectively. The TGA data of the SAN/

MMT/C16 series and SAN/MMT/P16 series nanocomposites are listed in Table 3. The TGA curves show that the SAN/clay nanocomposites exhibit better thermal stability than the pure SAN, namely delayed thermal decomposition and lower mass loss rate. The TGA data also show that all samples have a slightly early onset of decomposition. The reasons may be that the residual (excess) cationic surfactants on the silicate clay surface is thermal instability and undergoes a Hoffman degradation reaction, and its product would catalyze the degradation of polymer matrix. Moreover, it also may be due to the clay itself, which can also catalyze the degradation of polymer matrix [7, 25–27]. As far as the SAN/MMT/C16 series and the SAN/MMT/P16 series nanocomposites are concerned, the  $T_{-5 \text{ wt}\%}$  of SAN/MMT/C16 series nanocomposites decrease more than that of the SAN/MMT/P16 series nanocomposites, the probable reason is that the thermal stability of the P16 is higher than that of C16. Furthermore, the  $T_{-5 \text{ wt}\%}$  and the amount of char residue decrease and increase with the increase of the reactive compatibilizer content, respectively. Although the onset of weight loss of the SAN/clay nanocomposites occur at a lower temperature than that of the pristine SAN, all SAN/clay nanocomposites give a higher half weight loss temperature ( $T_{-50 \text{ wt}\%}$ ) and a larger char residue at 700 °C. The TGA data also indicate that the  $T_{-50 \text{ wt}\%}$  of the SAN/clay nanocomposites increase compared with the pristine SAN and the SAN/clay nanocomposites with 5 wt% MMT and 3 wt% reactive compatibilizer (C16 or P16) improve more notably. When the reactive compatibilizer content increase up to 5 wt%, the  $T_{-5 \text{ wt}\%}$  of the SAN/clay nanocomposites (SAN6 and SAN9) decrease remarkably, the reasons are explained in above paragraphs. A remarkable thermal stability effect is found for the polymer/clay nanocomposites and is likely to be due to an ablative reassembling of the silicate layers, which may occur on the surface of the polymer/clay nanocomposites creating a physical protective barrier on the surface of the material

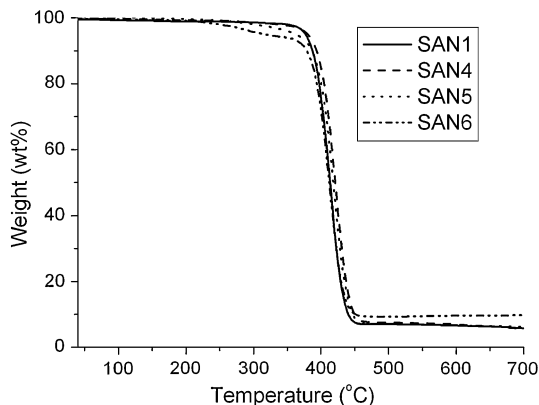


**Fig. 9** The TGA curves for SAN1, SAN4, SAN5 and SAN6

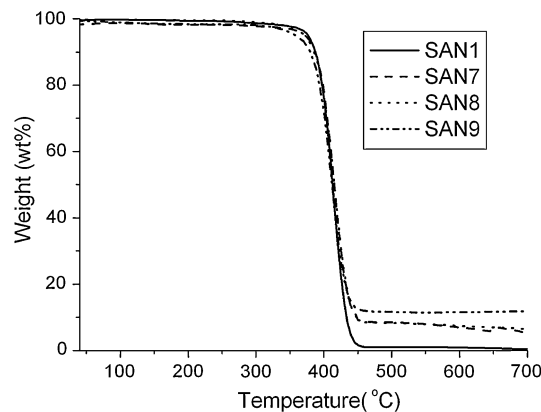


**Fig. 10** The TGA curves for SAN1, SAN7, SAN8 and SAN9

[28]. Volatilization might also be delayed by the labyrinth effect of the silicate layers dispersed in the polymer/clay nanocomposites.

Effect of two different process techniques on clay dispersion and properties of the SAN/clay nanocomposites

The effect of the different process techniques on the clay dispersion and properties is also studied. The TEM images indicate that the clay dispersion of SAN5 (Fig. 3d) is better than that of SAN3 (Fig. 3b). The reasons may be that the SAN/clay nanocomposites (containing MMT and C16) is a dynamically reactive process during melt-mixed. The prominent interaction will arise among the three components of the formulation: the silicate layer surface, the cationic surfactant chains (C16) and the polymer matrix. The detailed explanation is discussed above. However, there are not obvious differences as to thermal stability property. The char residue of the SAN/clay nanocomposites (containing MMT and C16) is higher than that of the SAN/clay nanocomposites (containing OMT) in SAN matrix. The cause may be related to the clay dispersion in the SAN matrix, contributing to the improved thermal stability. The storage modulus and Tg of the SAN/clay nanocomposites (SAN3 and SAN5) are shown in Figs. 6 and 7, respectively. There is a 44% and 137% enhancement in storage modulus at 30°C for SAN3 and SAN5 compared with the pristine SAN, respectively. The increase of storage modulus is strongly related with the solidlike properties of polymer/clay nanocomposites [6]. Compared with the OMT, the dynamically reactive process can promote the well-dispersed layers and cause to the solidlike behavior more highlighted in the presence of the MMT and C16. The morphology of the SAN3 and SAN5, respectively is intercalated and delaminated–intercalated structure. It is well known that the mechanical properties of the nanocomposites are enhanced relative to those of the

pristine polymers and that delaminated nanocomposites are enhanced relative to intercalated system [4]. However, The  $T_g$  of the SAN5 (111 °C) is lower than the SAN3 (113 °C). The decrease of the  $T_g$  is considered to be arisen due mainly to the excessive cationic surfactant (C16) exists in the SAN matrix. The plasticizing effect of the excessive C16 leads to the drop of  $T_g$  [29, 30]. Moreover, the SAN/clay nanocomposites (containing MMT and reactive compatibilizer) provide a simple and applied approach for manufacturing polymer–clay layered silicate nanocomposites.

#### Mechanism of intercalation

Ishida et al. [31] have reported the use of epoxy as the swelling agent of polymer/organoclay hybrids. In this paper, reactive compatibilizer (C16 and P16) serves to modify the clay layers, as well as to swell the clay layers. We deduce the mechanism: at the process of melting, where, at first, the reactive compatibilizers diffuses to the round of clay layers, and then through static adsorption and shear stress some reactive compatibilizer molecules intercalate into the silicate layers and expand them. Meanwhile, the reactive compatibilizer molecules can act as a carrier to transport the chains of matrix into the interlayer of clay during the melt-mixing process. The scheme of intercalation mechanism has been shown in Fig. 11.

#### Conclusion

The SAN/clay series nanocomposites are prepared by melt intercalation method originating from the pristine MMT and the organic modified MMT. The influences of two different silicate clays, reactive compatibilizer types and its loadings on nanocomposites formation, morphology, thermal and mechanical properties are carried out. It is found that the SAN cannot intercalate into the layers of MMT and results in microcomposites, then the intercalated structure is formed for the SAN nanocomposite containing OMT. The SAN/clay nanocomposites give the best clay dispersions in polymer matrix starting from the MMT and the reactive compatibilizers, since the system is a dynamically reactive process among MMT, reactive compatibilizers and SAN during melt-mixed. Furthermore, the appropriate proportion with 3 wt% reactive compatibilizers relative to 5 wt% MMT induces well-dispersed morphology and properties in the SAN matrix. The TGA analysis showed that all of the SAN/clay nanocomposites exhibit better thermal stability showing delayed thermal decomposition and lower mass loss rate than the pristine SAN. The dynamic mechanical analysis results show that the storage modulus and  $T_g$  of the SAN/clay nanocomposites increase

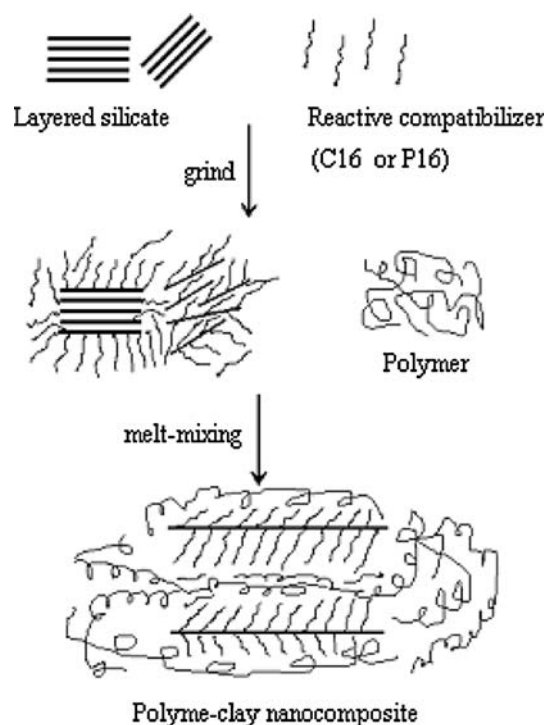


**Fig. 11** The scheme of intercalation mechanism

remarkably compared with the pristine SAN, due to the solidlike behavior of polymer/clay nanocomposites. At last the supposed intercalation mechanism of the technology has been studied. This work also shows that SAN/clay nanocomposites with better properties and simple technique process can be prepared, which provides a general concept for manufacturing other polymer/clay nanocomposites by direct melt intercalation.

**Acknowledgements** The work was financially supported by the National Natural Science Foundation of China (No. 50476026), Specialized Research Fund for the Doctoral Program of Higher Education (20040358056) and Program for New Century Excellent Talents in University.

#### References

1. Gilman JW, Jakson CL, Morgan AB, Harris RH, Manias E, Giannelis EP, Wuthenow M, Hilton D, Philips SH (2000) *Chem Mater* 12:1866
2. Devaux E, Bourbigot S, El Achari A (2002) *J Appl Polym Sci* 86:2416
3. Lan T, Kaviratna PD, Pinnavaia TJ (1994) *Chem Mater* 6:573
4. Alexander M, Dubois P (2000) *Mater Sci Eng* 28:1
5. Kim TH, Jang LW, Lee DC, Choi HJ, Jhon MS (2002) *Macromol Rapid Commun* 23:191
6. Lim ST, Lee CH, Choi HJ, Jhon MS (2003) *J Polym Sci Polym Phys* 41:2052
7. Chu LL, Anderson SK, Harris JD, Beach MW, Morgan AB (2004) *Polymer* 45:4051
8. Bourbigot S, Vanderhart DL, Gilman JW, Bellayer S, Stretz H, Paul DR (2004) *Polymer* 45:7627

9. Bok NJ, Wilie CA (2005) *Polymer* 46:9702
10. Stretz HA, Paul DR, Li R, Keskkula H, Cassidy PE (2005) *Polymer* 46:2621
11. Kim JW, Choi HJ, Jhon MS (2000) *Macromol Symp* 155:229
12. Kim JW, Jang LW, Choi HJ, Jhon MS (2003) *J Appl Polym Sci* 89:821
13. Wang HW, Chang KC, Chu HC (2005) *Polym Int* 54:114
14. Alexander M, Beyer G, Henrist C, Cloots R (2000) *Chem Mater* 13:3830
15. Kawasumi M, Hasegawa N, Kato M, Usuki A, Okada A (1997) *Macromolecules* 30:6333
16. Hasegawa N, Kawasumi M, Kato M, Usuki A, Okada A (1998) *J Appl Polym Sci* 67:87
17. Noh MH, Jang LW, Lee DC (1999) *J Appl Polym Sci* 74:179
18. Vaia RA, Giannelis EP (1997) *Macromolecules* 30:7990
19. Vaia RA, Teukoisky RK, Giannelis EP (1994) *Chem Mater* 6:1017
20. Tang Y, Hu Y, Wang JZ (2004) *J Appl Polym Sci* 91:2416
21. Anna CB, Chandralekha S (1998) *Macromolecules* 31:8370
22. Yulia L, Anna CB (1998) *Macromolecules* 31:6676
23. Valeriy VG, Chandralekha S, Anna CB (2000) *Macromolecules* 33:1089
24. Vaia RA, Giannelis EP (1997) *Macromolecules* 30:8000
25. Xie W, Xie R, Pan WP, Hunter D, Koene B, Tan LS, Vaia R (2002) *Chem Mater* 14:4837
26. Gilman JW, Awad WH, Davis RD, Shields J (2002) *Chem Mater* 14:3776
27. Zhu J, Morgan AB, Lamelas FJ, Wilkie CA (2001) *Chem Mater* 13:3774
28. Gilman JW, Kashivagi TCL, Giannelis EP, Manias E, Lomakin S, Lichtenhan JD (1998) In: Le Bras M, Caniino G, Bourbigot S, Delobel R (eds) *Fire retardancy of polymers*. The Royal Society of Chemistry, Cambridge
29. Choi YS, Xu MZ, Chung IJ (2003) *Polymer* 44:6989
30. Choi YS, Choi MH, Wang KH, Kim SO, Kim YK, Chung IJ (2001) *Macromolecules* 34:8978
31. Ishida H, Campbell S, Blackwell J (2000) *Chem Mater* 12:1260